



HAL
open science

All-optical isotropic scalar 4He magnetometer based on atomic alignment

G. Lieb, T. Jager, A. Palacios-Laloy, H. Gilles

► **To cite this version:**

G. Lieb, T. Jager, A. Palacios-Laloy, H. Gilles. All-optical isotropic scalar 4He magnetometer based on atomic alignment. *Review of Scientific Instruments*, 2019, 90 (7), pp.075104. 10.1063/1.5093533 . hal-04318636

HAL Id: hal-04318636

<https://hal.science/hal-04318636v1>

Submitted on 12 Nov 2024


HAL is a multi-disciplinary open access archive for the deposit and dissemination of scientific research documents, whether they are published or not. The documents may come from teaching and research institutions in France or abroad, or from public or private research centers.

L'archive ouverte pluridisciplinaire **HAL**, est destinée au dépôt et à la diffusion de documents scientifiques de niveau recherche, publiés ou non, émanant des établissements d'enseignement et de recherche français ou étrangers, des laboratoires publics ou privés.

All-optical isotropic scalar ^4He magnetometer based on atomic alignment

EP

Cite as: Rev. Sci. Instrum. **90**, 075104 (2019); <https://doi.org/10.1063/1.5093533>
 Submitted: 21 February 2019 . Accepted: 27 May 2019 . Published Online: 08 July 2019

G. Lieb, T. Jager, A. Palacios-Laloy , and H. Gilles

COLLECTIONS

 This paper was selected as an Editor's Pick



View Online



Export Citation



CrossMark

ARTICLES YOU MAY BE INTERESTED IN

[Time-resolved laser-induced desorption spectroscopy \(LIDS\) for quantified in-situ hydrogen isotope retention measurement and removal from plasma facing materials](#)
 Review of Scientific Instruments **90**, 073502 (2019); <https://doi.org/10.1063/1.5100162>

[Development of a compact tunable diode laser absorption spectroscopy based system for continuous measurements of dissolved carbon dioxide in seawater](#)
 Review of Scientific Instruments **90**, 065110 (2019); <https://doi.org/10.1063/1.5095797>

[High sensitivity microwave spectroscopy in a cryogenic buffer gas cell](#)
 Review of Scientific Instruments **90**, 053104 (2019); <https://doi.org/10.1063/1.5091773>

Lock-in Amplifiers
up to 600 MHz



All-optical isotropic scalar ^4He magnetometer based on atomic alignment

Cite as: Rev. Sci. Instrum. **90**, 075104 (2019); doi: [10.1063/1.5093533](https://doi.org/10.1063/1.5093533)

Submitted: 21 February 2019 • Accepted: 27 May 2019 •

Published Online: 8 July 2019




View Online



Export Citation



CrossMark

G. Lieb,¹ T. Jager,¹ A. Palacios-Laloy,^{1,a)}  and H. Gilles²

AFFILIATIONS

¹CEA-Leti, MINATEC Campus, F-38054 Grenoble, France and University of Grenoble Alpes, F-38000 Grenoble, France

²CIMAP, UMR 6252 CNRS, CEA, ENSICAEN, Normandie Université, Boulevard Marechal Juin, F-14050 Caen, France

^{a)}Electronic mail: agustin.palacioslaloy@cea.fr

ABSTRACT

We propose a helium scalar magnetometer based on a triple resonance setup, showing no dead angles, and which can be implemented in an all-optical way. This *triple-resonance* scheme involves optical pumping with amplitude-modulated light, complemented by a modulated light-shift. Both light beams propagate parallel so that a single optical access to the atomic cell is needed. Experimental results are in good agreement with our theoretical model. The main error sources affecting the magnetometer accuracy are discussed.

Published under license by AIP Publishing. <https://doi.org/10.1063/1.5093533>

I. INTRODUCTION

Accurate measurements of the local magnetic field are crucial for geomagnetic mapping,¹ field measurements in space,² Magnetic Anomaly Detection (MAD), and searches for permanent electric dipole moments.^{3,4} Magnetic resonance phenomena provide unprecedented levels of accuracy for these measurements, thanks to the absolute character of the physical principle involved, and its immunity to aging and temperature drifts. These phenomena were first instrumented in NMR (Nuclear Magnetic Resonance) magnetometers which have become widespread scalar reference instruments.⁵

Developed in the 1960s, optical pumping of diluted atomic gasses⁶ opened the way to a new generation of magnetic resonance magnetometers.⁷ In these scalar optically pumped magnetometers (OPMs), electronic spins of an atomic gas are first prepared in a state characterized by a magnetic moment by using light and resonant with a well-chosen transition.⁶ Then the magnetic resonance between the Zeeman sub-levels is excited by a radio-frequency (RF) field. The resulting atomic state is monitored by optical means, for instance, by measuring the absorption of the pump light. These double resonance (light + RF) magnetometers outperform the NMR ones in several ways: they provide larger bandwidth, much lower noise, improved electromagnetic compatibility⁸ with at least the same accuracy level.

However, due to the symmetry breaking by the polarization of the pumping light, all optically pumped magnetometers show dead

zones, where they are unable to measure the field because the resonance signal vanishes. The suppression of these dead zones is very desirable, especially for applications where the sensor is mobile, such as Earth navigation or space exploration. Several ways to overcome this issue have been proposed and operated, notably the combination of several magnetometers showing complementary dead zones, which is, however, cumbersome and highly sensitive to gradients. In the 1990s, the CEA-Leti pioneered an isotropic architecture based on locking the linear polarization of the pump light orthogonal to the measured magnetic field⁹ with a servo loop. Since November 2013, magnetometers based on this principle are successfully operated on board the satellites of the European Space Agency (ESA) Swarm mission.¹⁰

In parallel, aiming for simpler and lighter magnetometers, efforts were made for replacing the coil-generated RF field by a modulation of the pumping light. These efforts sought to extend the seminal work of Bell and Bloom¹¹ on all-optical Mx magnetometer to other configurations. Various architectures based on Amplitude Modulation (AM),^{12,13} Frequency Modulation (FM),^{13,14} and Polarization Modulation (PM)^{13,15–18} of the pump light have been proposed and tested. A recent work¹⁹ presents an interesting although complex dead-zone free scheme analog to CEA-Leti's one consisting in an AM pump combined with a slow PM. Another approach consists in replacing RF by a modulated nonresonant light, resulting in time-varying vector light-shifts, yielding an oscillating fictitious magnetic field.^{20,21} This scheme, however, shows dead zones.

In this paper, we study another scheme with suppressed dead zones. We show that combining double resonance and pump modulation could lead to a new *triple-resonance magnetometer* whose architecture presents an operation point very similar to the CEA-Leti architecture. This scheme can be implemented in an all-optical configuration combining a resonant AM pump with an AM circularly polarized beam which creates a light-shift RF field. Both beams propagate parallel which allows using a single optical access to the gas cell. This scheme opens the way to a compact isotropic all-optical scalar magnetometer.

II. ALIGNMENT-BASED SCALAR MAGNETOMETERS AND ISOTROPY

Most of isotropic scalar magnetometers are based on atomic alignment. In the same way, as atomic orientation involves a non-null average spin projection $\langle S_k \rangle$ along some axis k , atomic

alignment is defined by non-null second-order moment $3\langle S_k \rangle^2 - \langle S^2 \rangle$. Alignment can be created in any spin ≥ 1 : we will consider helium 4 in its 2^3S_1 metastable level, a spin one. This level has three Zeeman substates characterized by their spin projection along a given direction $m = -1, 0, 1$. The population of these sublevels can be prepared by depopulation optical pumping with 2^3P_0 level.²²

Figure 1(a) presents the simplest alignment-based scalar magnetometer architecture. The ambient field B_0 to be measured fulfills the condition $\gamma B_0 \gg \Gamma$, where $\gamma = -2\pi \times 28$ rad/s/nT is the gyromagnetic ratio and Γ is the relaxation rate of metastable level (typically 10^3 – 10^4 Hz). A RF field $B_{RF} \cos(\omega t)$ at angular frequency ω near the Larmor frequency $\omega_L = \gamma B_0$ excites the magnetic resonance. When ω lies in the near vicinity of ω_L , three resonances appear: around null frequency, around ω , and around 2ω . The amplitudes of these resonances depend on the angle β between the magnetic field and the light polarization, as calculated by Weis *et al.*²³ and shown in Fig. 1(a).

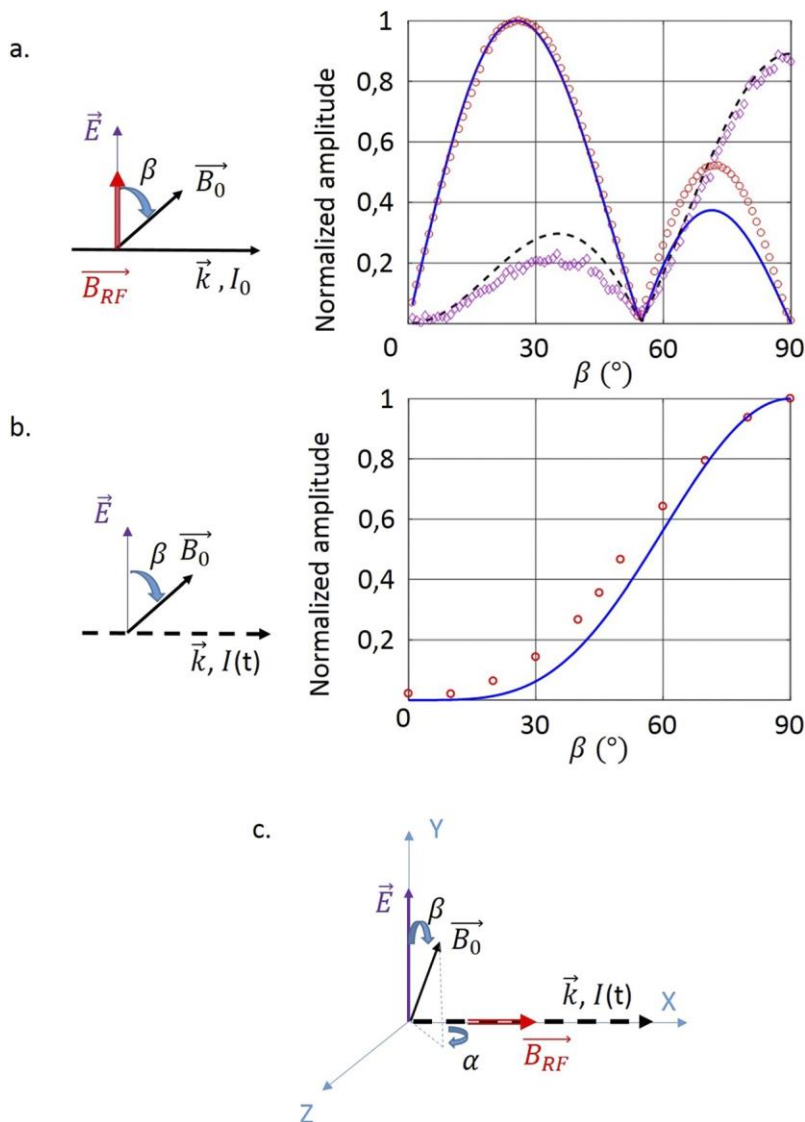


FIG. 1. Geometrical descriptions and amplitude anisotropy of different scalar magnetometer schemes. (a) RF magnetometer; solid blue line: amplitude isotropy of the resonance signals at ω , black dashed line: the one at 2ω , red circles: experimental results at ω obtained with light-shift RF, purple diamonds: the ones at 2ω ; (b) magnetometer with AM pump at 2ω with $I(t) = I_0(1 + \cos(2\omega t))$; solid blue line: amplitude isotropy at 2ω , red circles: experimental results at 2ω ; and (c) triple-resonance magnetometer with $I(t) = I_0(1 + \cos(2\omega t))$.

Guttin *et al.*⁹ demonstrated that an isotropic magnetometer can be obtained by locking the polarization to $\beta = \pi/2$. This condition can be stabilized by rotating the light polarization with an amagnetic motor²⁴ or a polarization rotator.²⁵ The error signal for this lock is provided by the odd parity in β of the resonance at ω . The field measurement can be performed by locking ω at resonance with ω_L using the 2ω signal [Fig. 1(a)].

Scalar magnetometers can also be obtained without RF field by modulating the pump intensity, as presented in Fig. 1(b).¹² In this case, a resonance is observed when pumping light is modulated in amplitude at an angular frequency $\omega \approx 2\omega_L$. The amplitude of this resonance as a function of β is presented on the right side of Fig. 1(b). A response at 4ω with the same dependence is also present.²⁶ None of these resonance signals presents the odd parity required to lock β as previously described.

An isotropic configuration could be obtained if it was possible to combine the angular dependency of the resonance at ω obtained in the RF scheme with one of the resonance at 2ω obtained in the AM pump scheme. This suggested us to study the scheme displayed on Fig. 1(c) which combines an amplitude-modulated pump at 2ω with an RF field at ω colinear to light propagation. We will show theoretically in Sec. III and experimentally in Sec. IV that this configuration yields to signals with the requested characteristics to build an isotropic magnetometer. We will explain in Sec. V how this RF field colinear to light propagation could be generated by using light-shift. Note that in this scheme, a second angle α is needed to accurately describe the geometry, as shown in Fig. 1(c).

III. THEORY OF TRIPLE-RESONANCE MAGNETOMETER

The collective state of atoms in the helium-4 2^3S^1 metastable level can be described by a 3×3 density matrix ρ . For magnetometry, it is useful to decompose it on magnetic multipoles basis^{27,28}

$$\rho = \sum_{k=0}^{2F} \sum_{q=-k}^k m_q^{(k)} T_q^{(k)\dagger}. \quad (1)$$

Since helium-4 atoms are pumped with linearly polarized light, only $k = 0, 2$ are populated. In the following, we will restrict our analysis to alignment ($k = 2$), which can be described by the five-components column matrix $M = (m_2^{(2)} \ m_1^{(2)} \ m_0^{(2)} \ m_{-1}^{(2)} \ m_{-2}^{(2)})^t$.

Atoms are subject to the pumping light, which acts also as a probe, and to a magnetic field comprising static and RF components. As long as the pumping light intensity is low, the evolution can be

modeled by the following equation:^{23,29}

$$\left[\frac{d}{dt} - H(\vec{B}, \tau) + \Gamma(t) \right] M = \Gamma(t) M_{ss}. \quad (2)$$

The right-hand side corresponds to linearly polarized pumping, which makes alignment evolve toward the steady-state $M_{ss} = m_{ss}(0 \ 0 \ 1/6 \ 0 \ 0)^t$, where m_{ss} is a constant depending on pumping power and on atomic relaxation. This steady-state is written with the quantization axis along the E field of the pumping light. The total relaxation $\Gamma(t)$ includes the relaxation in the dark as well as the relaxation brought by the pumping, which in our case is time dependent due to the light modulation, yielding $\Gamma(t) = \Gamma_0(1 + \cos(2\omega t))$. The left-hand side comprises the evolution under the total magnetic field $\vec{B}_0 + \vec{x}B_{RF} \cos(\omega t + \varphi)$ which is described using the 5×5 matrix $H(\vec{B}, \tau)$ as introduced in the work of Weis *et al.*²³ under the name O_{qq}^2 . Equation (2) becomes much simpler when rewritten with quantization axis along the magnetic field. This change of the frame is obtained by premultiplying M by the Wigner-D matrix²⁸ $D^2(0, \beta, \alpha)$, where α, β are the angles of Fig. 1(c). Moving to the frame rotating at angular frequency ω around B_0 , the alignment M becomes $M' = D^2(0, 0, -\omega t)M$, yielding

$$\frac{d}{dt} M' = -i \begin{pmatrix} -2\delta & \omega_1 e^{-i\varphi} & \sqrt{3}/2 & 0 & 0 \\ \omega_1 e^{i\varphi} & -\delta & \sqrt{3}/2 \omega_1 e^{-i\varphi} & 0 & 0 \\ 0 & \sqrt{3/2} \omega_1 e^{i\varphi} & 0 & \sqrt{3/2} \omega_1 e^{-i\varphi} & 0 \\ 0 & 0 & \sqrt{3/2} \omega_1 e^{i\varphi} & \delta & \omega_1 e^{-i\varphi} \\ 0 & 0 & 0 & \omega_1 e^{i\varphi} & 2\delta \end{pmatrix} M' + \Gamma_0 [M'_{ss} - M'], \quad (3)$$

where $\delta = \omega - \gamma B_z$ and $\omega_1 = \gamma B_{RF}(1 - \sin^2(\beta) \cos^2(\alpha))^{1/2}$, the component of \vec{B}_{RF} being transverse to B_0 with the angles of Fig. 1(c). The pumping steady state in this rotating frame M'_{ss} is obtained by decomposing in Fourier series the time evolution of the pumping. Since the component $m_q^{(2)}$ rotates at $q\omega$ angular frequency in the lab frame, only the Fourier component q should affect the component $m_q^{(2)}$, yielding in our case $m_{\pm 2,ss}^{(2)} = m_{\pm 2}^{(2)}/2$, $m_{\pm 1,ss}^{(2)} = 0$, and $m_{0,ss}^{(2)} = m_0^{(2)}/2$. In the secular approximation $dM'/dt \approx 0$, Eq. (3) leads to an algebraic equation which can be solved using appropriate software, for instance, Mathematica. We thus obtain the following anisotropy $S_\omega(\alpha, \beta)$ and $S_{2\omega}(\alpha, \beta)$ for the signals at ω and 2ω respectively,

$$S_\omega(\alpha, \beta) = -\frac{\sqrt{3}}{2} \frac{\omega_1(\alpha, \beta) \sin(\beta) \cos(\beta) [(6\omega_1^2(\alpha, \beta) - 9) \cos(2\beta) + 10\omega_1(\alpha, \beta)^2 + 1]}{64(4\omega_1(\alpha, \beta)^4 + 5\omega_1(\alpha, \beta)^2 + 1)}, \quad (4)$$

$$S_{2\omega}(\alpha, \beta) = \frac{\sqrt{3} \sin^2(\beta) [(13\omega_1(\alpha, \beta)^2 - 2) \cos(2\beta) + 11\omega_1(\alpha, \beta)^2 + 2]}{2 [64(4\omega_1(\alpha, \beta)^4 + 5\omega_1(\alpha, \beta)^2 + 1)]}. \quad (5)$$

$S_\omega(\alpha, \beta)$ and $S_{2\omega}(\alpha, \beta)$ are shown in Fig. 2. Figure 2(b) shows that for every α , the signal goes through zero at $\beta = 90^\circ$. This corresponds to one of its components changing sign at $\beta = 90^\circ$. Figure 2(c) shows that the signal at 2ω is non-null at $\beta = 90^\circ$ for any α . It even happens to be maximal at this point. This allows us to

measure B_0 with an optimal sensitivity while locking the condition $\beta = 90^\circ$, as described in Sec. II.

In order to estimate the sensitivity of this triple-resonance scheme, we have compared the theoretical slopes resulting from this calculation to those of the isotropic double-resonance scheme. If we

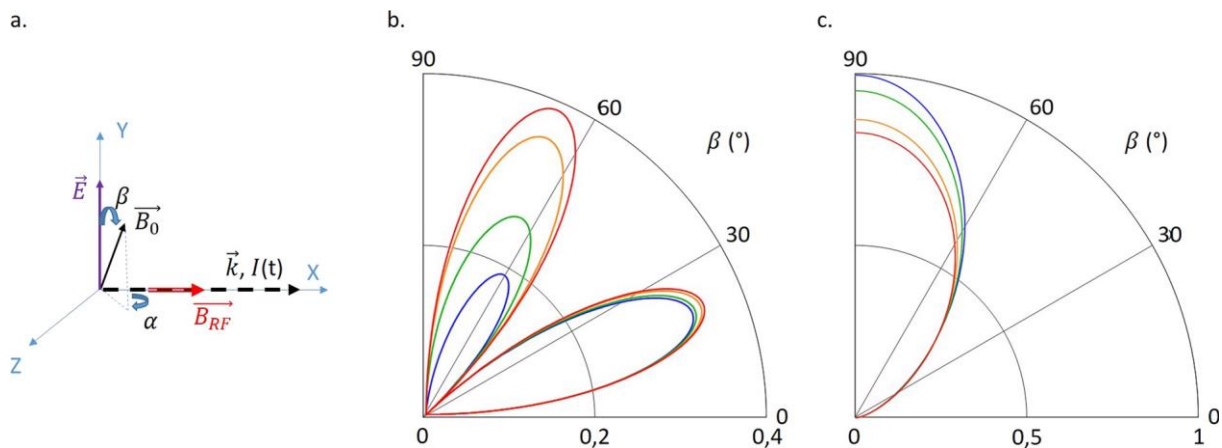


FIG. 2. Theoretical predictions for the amplitude anisotropy of the triple resonance magnetometer; (a) geometrical description of the architecture; (b) theoretical amplitude of the resonance at ω ; (c) theoretical amplitude of the resonance at 2ω . All signals are normalized by the maximum amplitude of 2ω signal; red: $a = 90^\circ$, orange: $a = 60^\circ$, green: $a = 30^\circ$, and blue: $a = 0^\circ$.

consider an isotropic distribution of a , both slopes match closely. Since the double-resonance isotropic scheme was demonstrated¹⁰ to reach $1 \text{ pT/Hz}^{1/2}$, this same sensitivity should be achievable with the triple-resonance one.

IV. EXPERIMENTAL CHARACTERIZATION OF THE AMPLITUDE ANISOTROPY

In order to verify the above predictions, we built the experimental setup shown in Fig. 3(b). A cylindrical cell of 10 mm diameter and 10 mm length filled with 30 Torr of helium is used. The metastable level is populated by an AC discharge at 6.72 MHz frequency absorbing 70 mW power. A linearly polarized light beam of 12 mm waist propagates along the longitudinal axis of the cell. The beam intensity is modulated using an acousto-optical modulator from AA Optoelectronic (MT110-IR20-FIO). The RF field is generated using coils. A 140 kHz frequency, corresponding to the Larmor frequency of a $5 \mu\text{T}$ magnetic field, and an amplitude of 11 nT were chosen. The pumping laser is a distributed feedback (DFB) diode from the QD laser at 1083 nm. The light transmitted through the cell is photodetected with a photodetector (TIA 525I from Terahertz Technologies Inc.), and signals are processed by a lock-in amplifier (LIA) (SR865A from Stanford).

In order to study the amplitude anisotropy, a magnetic field \vec{B}_0 of controlled direction is generated thanks to three Helmholtz coils (accuracy of 10^{-3} , orthogonality better than 2 mrad) enclosing the cell, as depicted in Fig. 3(b). For each magnetic field direction (α , β), the resonance signals are acquired and fitted allowing a precise derivation of both the amplitudes and the slopes at resonance.

Figure 3(c) shows that for any a , the amplitude of the signal at ω goes to zero at $\beta = 90^\circ$. Moreover Fig. 3(e) shows that the in-phase component of this signal changes sign, as predicted by theory. This confirms that the signal can be used for the polarization locking. At the same time for any angle a , the signal at 2ω is not null at $\beta = 90^\circ$ as shown in Fig. 3(d) and so it can be used to measure the magnetic field. The signal at 2ω is even maximal at $\beta = 90^\circ$ which is

optimal in terms of resolution for the field measurement. The most visible disagreement with the theoretical results is the nonexplained inversion of the curves for $a = 60^\circ$ and $a = 90^\circ$.

This confirms that triple resonance technique allows us to obtain an isotropic magnetometer. Furthermore, the RF field generated thanks to coils could be obtained by using a modulated light-shift generated by a beam sent through the same optical access as the pump beam.

V. FICTITIOUS RF FIELD IMPLEMENTED WITH A MODULATED LIGHT-SHIFT

The possibility of implementing scalar magnetometers using modulated light-shifts in replacement of electrical RF was demonstrated in the past.²¹ Parametric resonance magnetometers have also been implemented in this way.^{30,31}

Light-shift consists in a displacement of the Zeeman sublevels caused by a circularly polarized light detuned from the optical resonance line, here the D_0 pumping line at 1083.206 nm. This displacement is equivalent to a fictitious magnetic field \vec{B}_{LS} colinear to the beam propagation. For metastable, helium subject to a purely circularly polarized beam its amplitude writes³²

$$B_{LS} = \frac{3}{8} \frac{\pi r_e c \phi}{\gamma} \mathbb{I}[2f_{D_0} V(\nu - \nu_0) + f_{D_1} V(\nu - \nu_1) - f_{D_2} V(\nu - \nu_2)], \quad \text{€}$$

where ϕ is the photon flux, r_e is the classical electron radius, c is the speed of light, V is the Voigt profile, $\nu - \nu_i$ and f_{D_i} are the detuning of light and the oscillator strength of D_i line, respectively.³³

We first performed an experimental measurement of B_{LS} as a function of the wavelength to verify that the fictitious field can reach the amplitude required for RF. Figure 4(a) shows the corresponding setup with a laser beam propagating parallel to the static field. By varying its wavelength, the magnetic resonance can be shifted. As it is presented in Fig. 4(b), the generated B_{LS} amplitude measured from the resonance detuning is in good agreement with theory.

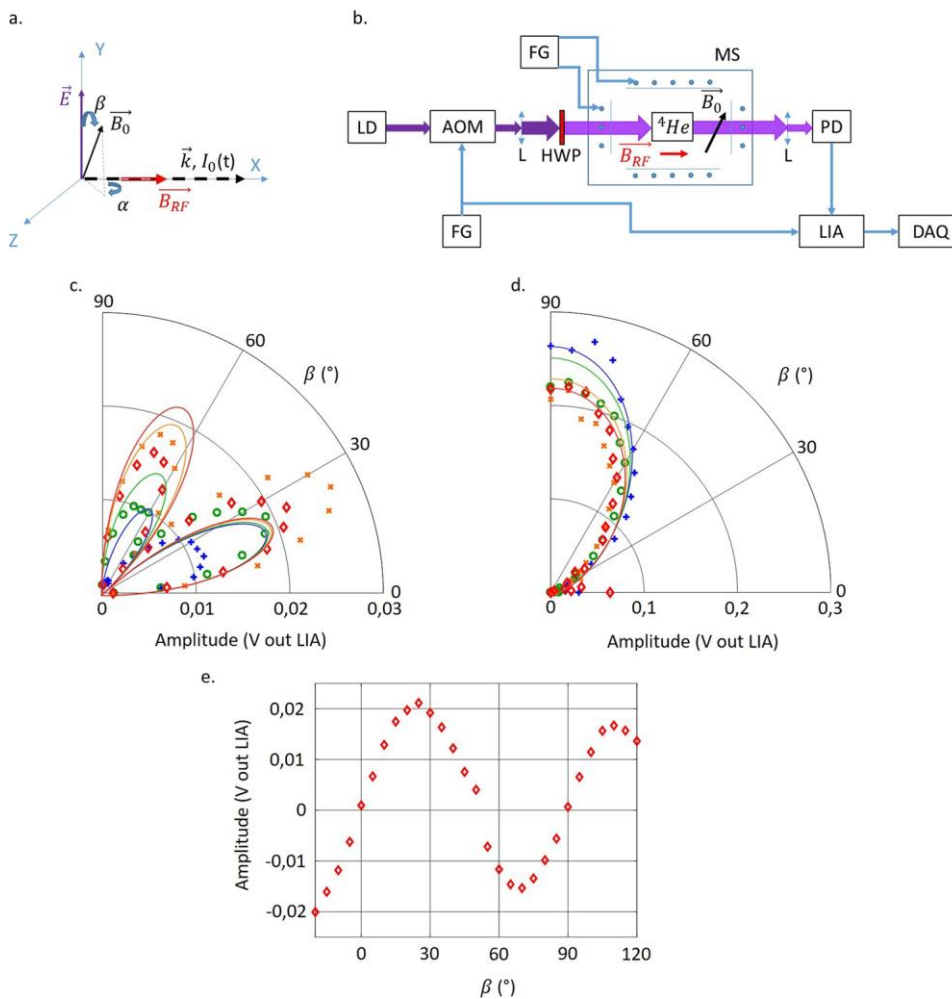


FIG. 3. Experimental characterization of the amplitude anisotropy of the triple-resonance magnetometer. (a) Triple resonance magnetometer scheme; (b) experimental setup, LD laser diode, AOM acousto-optic modulator, L lens, HWP half-wave-plate, MS magnetic shield, PD photodiode, LIA Lock-in amplifier, FG function generator, and DAQ data acquisition. Amplitude anisotropy of the magnetometer for signals at (c) the Larmor frequency and (d) twice the Larmor frequency. (e) Angular dependence of in-phase component measured at the Larmor frequency; red diamonds: $\alpha = 90^\circ$, orange crosses: $\alpha = 60^\circ$, green circles: $\alpha = 30^\circ$, and blue crosses: $\alpha = 0^\circ$. Solid lines are theoretical predictions given in the text.

A drawback of using light-shift for applying fictitious magnetic fields is the residual absorption of this beam, which causes spurious pumping of the atoms. In order to determine the highest amplitude of magnetic field which can be generated before the light-shift beam overcomes nominal pumping, we computed for each λ , B_{LS} corresponding to broadening of resonance by a factor 2. As shown in Fig. 4(c), a large enough field (i.e., superior to 80 nT) can be obtained. The optimal wavelength is around 1083.250 nm, where the feet of D_1 and D_2 make the accessible light-shift higher than at 1083.500 nm, while allowing us to use less laser intensity than at 1083.150 nm.

By modulating the beam intensity, it is possible to generate a fictitious oscillating field, i.e., the RF. In order to probe if this fictitious RF field is equivalent to a coil-induced RF field, we measured the angular dependence of the magnetic resonance signals. Light-shift beam is amplitude modulated with an acousto-optical modulator (same model as previously described) with a sinusoidal peak-to-peak modulation ranging from 0 to 6 mW, which corresponds to a time-varying magnetic field between 0 and 12 nT. When the modulation frequency matches the Larmor frequency of the

static field (140 kHz–5 μ T), magnetic resonance signals are observed. In Fig. 1(a), the amplitudes of these signals are compared to the theoretical expectations for a coil-based scalar magnetometer. There is an excellent agreement between both, showing that the LS-based RF acts in the very same way as coil-induced RF.

VI. MAIN MECHANISMS OF FREQUENCY ANISOTROPY

Beside amplitude anisotropy characteristics, scalar magnetometers can show frequency anisotropy which affects their accuracy. Any phenomenon shifting the magnetic resonance frequency, and showing an angular dependence, causes such an anisotropy. For instance, the feet of the resonance signal at ω may result in an apparent shift of the center of the resonance at 2ω . Since both signals show angular dependences, this is a potential source of frequency anisotropy. However, as discussed elsewhere in the work of Gutin *et al.*,³⁴ this shift disappears when locking β at 90° . We will discuss here about 2 important effects which cause frequency anisotropies: the anisotropy of Bloch-Siegert shift and the vector light-shift offset.

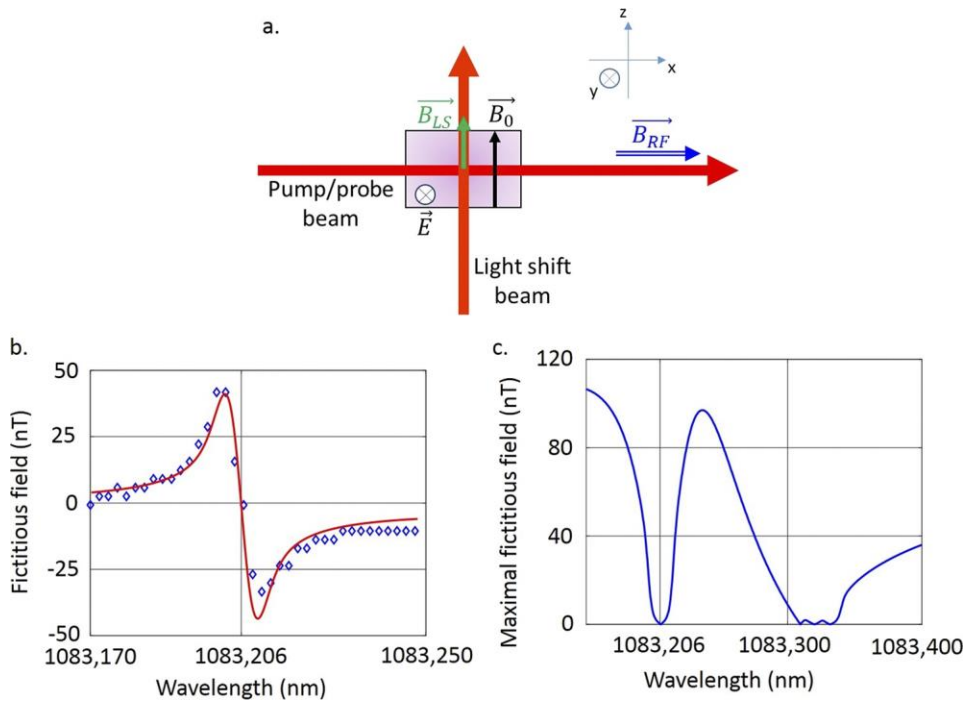


FIG. 4. Calibration of the amplitude of the fictitious field resulting from light-shift. (a) Scheme for light-shift measurement (laser beams are not at scale, they completely cover the cell in the actual setup). (b) In continuous line, the theoretical fictitious field amplitude generated by LS for a 5.5 mW light intensity, and in dot line, the experimental results. (c) The maximal fictitious field reachable before concurrencing the pumping light at the saturation.

A. Anisotropy of the Bloch-Siegert shift

As described by Bloch and Siegert,³⁵ exciting magnetic resonance with an oscillating RF field, instead of a rotating one, causes a shift in resonance frequency. This shift has a quadratic dependence with B_{RF} , the component of \vec{B}_{RF} transverse to \vec{B}_0 : $\Delta B_0 = B_{RF\perp}^2 / (4B_0)$ [cf. Fig. 5(a)].

Since the angle between \vec{B}_{RF} and \vec{B}_0 is not fixed, this shift becomes anisotropic. Figure 5(c) illustrates this particular dependence in the case of a 5 μ T field and $\beta = 90^\circ$.

The maximal amplitude of this anisotropy corresponds to the amplitude of the shift: for an ambient field of 5 μ T, the theoretical prediction is shown in Fig. 5(b) as a function of the transverse RF field. We experimentally characterized this dependence as shown in Fig. 5(b). With an 11 nT amplitude RF field, the maximal anisotropy due to the Bloch-Siegert effect is of 24.2 pT when $\alpha = 90^\circ$. If we want to operate this magnetometer in the Earth magnetic field varying between 15 and 55 μ T and with an RF of 100 nTpp, we are then expecting an anisotropy varying between ~170 pT and ~45 pT, respectively.

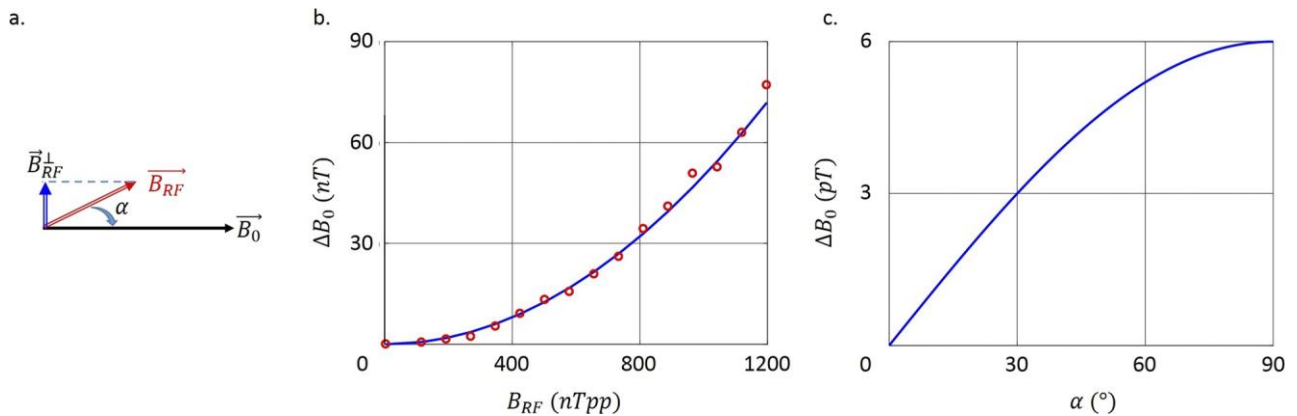


FIG. 5. Bloch-Siegert shift and the resulting frequency anisotropy for $\beta = 90^\circ$. (a) Geometrical configuration of the experiment, (b) Bloch-Siegert shift as a function of the RF amplitude, and (c) angular dependence of the shift.

B. Vector light-shift offset

As described in Sec. V, to build an all optical magnetometer, the RF field can be generated with an amplitude modulated light-shift. In this configuration, the mean value of the intensity of the light-shift beam is $I_{max}/2$. This non-null average intensity brings a field offset along the light propagation axis. For an 11 nT amplitude optical RF, the average intensity of light-shift beam is 5.5 mW. This means that in the worst case ($\alpha = 0^\circ$; $\beta = 90^\circ$), the offset is of 11 nT. This offset shows an angular $\cos(\alpha) \sin(\beta)$ dependence which creates anisotropy. However, this anisotropy can be suppressed by using a polarization modulation in addition to amplitude modulation. Indeed, σ^+ and σ^- polarizations bring opposite light-shifts allowing us to keep a null average light-shift. This kind of optical RF can be obtained by using a laser modulated in intensity with a $|\cos(2\omega t)|$ time dependence, and a σ^+ polarization for $\cos(2\omega t) > 0$ and a σ^- polarization for $\cos(2\omega t) < 0$.

VII. CONCLUSION AND PERSPECTIVES

The combination of a modulated pump and a modulated light-shift beam yields a triple-resonance magnetometer. We provide evidence that this scheme opens the way to an all-optical dead-zone free scalar magnetometer.

This scheme should be able to deliver sensitivities around 1 pT/Hz^{1/2}. Its accuracy is, however, degraded with respect to the isotropic double-resonance scheme due to the anisotropy of the Bloch-Siegert shift. In the most pessimistic setting, this contribution can reach 50 pT. Based on past measurement in space with double-resonance magnetometers,¹⁰ the overall accuracy should be below 100 pT at 1σ .

Further work on a complete implementation of this configuration, including all the light modulations and the control loops, will allow to probe experimentally the frequency anisotropy and its accuracy and to compare it with other isotropic scalar magnetometry schemes.

ACKNOWLEDGMENTS

We want to acknowledge technical support by W. Fourcault and C. Gobbo, cell filling by F. Alcouffe, and interesting discussions with S. Morales, F. Bertrand, and J. M. Leger. This work was supported by CEA LETI DSYS Ph.D. funding.

REFERENCES

- ¹M. Nabighian, V. Grauch, R. Hansen, T. LaFehr, Y. Li, J. Peirce, J. Phillips, and M. Ruder, *Geophysics* **70**, 33ND (2005).
- ²N. Olsen, G. Hulot, and T. J. Sabaka, *Space Sci. Rev.* **155**, 65 (2010).
- ³P. Knowles, G. Bison, N. Castagna, A. Hofer, A. Mtchedlishvili, A. Pazgalev, and A. Weis, *Nucl. Instrum. Methods Phys. Res., Sect. A* **611**, 306 (2009).
- ⁴S. Afach, C. A. Baker, G. Ban, G. Bison, K. Bodek, M. Burghoff, Z. Chowdhuri, M. Daum, M. Fertl, B. Franke, P. Geltenbort, K. Green, M. G. D. van der Grinten, Z. Grujic, P. G. Harris, W. Heil, V. Hélaine, R. Henneck, M. Horras, P. Iaydjiev, S. N. Ivanov, M. Kasprzak, Y. Kermaidic, K. Kirch, A. Knecht, H. C. Koch, J. Krempel, M. Kuz'niak, B. Lauss, T. Lefort, Y. Lemièrre, A. Mtchedlishvili, O. Naviliat-Cuncic, J. M. Pendlebury, M. Perkowski, E. Pierre, F. M. Piegsa, G. Pignol, P. N. Prashanth, G. Quémener, D. Rebreyend, D. Ries, S. Roccia, P. Schmidt-Wellenburg, A. Schnabel, N. Severijns, D. Shiers, K. F. Smith, J. Voigt, A. Weis, G. Wyszynski, J. Zejma, J. Zenner, and G. Zsigmond, *Phys. Lett. B* **739**, 128 (2014).
- ⁵S. Beguš and D. Fefer, *Meas. Sci. Technol.* **18**, 901 (2007).
- ⁶W. Happer, *Rev. Mod. Phys.* **44**, 169 (1972).
- ⁷A. Grosz, *High Sensitivity Magnetometers* (Springer, 2016).
- ⁸J.-M. Léger, IAC-11-B1.3.9, 6, 2011.
- ⁹C. Guttin, J. M. Leger, and F. Stoeckel, *Le J. Phys.* **IV 4**, C4-655 (1994).
- ¹⁰J.-M. Léger, T. Jager, F. Bertrand, G. Hulot, L. Brocco, P. Vigneron, X. Lalanne, A. Chulliat, and I. Fratter, *Earth, Planets Space* **67**, 57 (2015).
- ¹¹W. E. Bell and A. L. Bloom, *Phys. Rev.* **107**, 1559 (1957).
- ¹²H. Gilles, B. Cheron, and J. Hamel, *J. Phys.* **II 2**, 781 (1992).
- ¹³Z. D. Grujic' and A. Weis, *Phys. Rev. A* **88**, 012508 (2013); e-print [arXiv:1305.6574](https://arxiv.org/abs/1305.6574).
- ¹⁴B. Chéron, H. Gilles, J. Hamel, O. Moreau, and E. Noël, *Opt. Commun.* **115**, 71 (1995).
- ¹⁵H. Gilles, B. Cheron, and J. Hamel, *Opt. Commun.* **81**, 369 (1991).
- ¹⁶H. Gilles, B. Cheron, and J. Hamel, *J. Phys.* **IV 01**, C7 (1991).
- ¹⁷G. Bevilacqua and E. Breschi, *Phys. Rev. A* **89**, 062507 (2014).
- ¹⁸E. Breschi, Z. D. Grujic, P. Knowles, and A. Weis, *Appl. Phys. Lett.* **104**, 023501 (2014); e-print [arXiv:1312.3567](https://arxiv.org/abs/1312.3567).
- ¹⁹T. Wu, X. Peng, Z. Lin, and H. Guo, *Rev. Sci. Instrum.* **86**, 103105 (2015).
- ²⁰E. Zhivun, A. Wickenbrock, B. Patton, and D. Budker, *Appl. Phys. Lett.* **105**, 192406 (2014).
- ²¹B. Patton, E. Zhivun, D. C. Hovde, and D. Budker, *Phys. Rev. Lett.* **113**, 013001 (2014).
- ²²F. D. Colegrove and P. A. Franken, *Phys. Rev.* **119**, 680 (1960).
- ²³A. Weis, G. Bison, and A. S. Pazgalev, *Phys. Rev. A* **74**, 033401 (2006).
- ²⁴T. Jager, J.-M. Léger, F. Bertrand, I. Fratter, and J.-C. Lalaurie, in *2010 IEEE Sensors* (IEEE, 2010), pp. 2392–2395.
- ²⁵J. Rutkowski, "Study and realization of a miniature isotropic helium magnetometer," Ph.D. thesis, Franche-Comté, CEA-LETI-DRT Grenoble, 2014.
- ²⁶H. Gilles, J. Hamel, and B. Chéron, *Rev. Sci. Instrum.* **72**, 2253 (2001).
- ²⁷K. Blum, *Density Matrix Theory and Applications*, Springer Series on Atomic, Optical, and Plasma Physics Vol. 64 (Springer Berlin Heidelberg, Berlin, Heidelberg, 2012).
- ²⁸A. Omont, *Prog. Quantum Electron.* **5**, 69 (1977).
- ²⁹A. Weis, J. Wurster, and S. I. Kanorsky, *J. Opt. Soc. Am. B* **10**, 716 (1993).
- ³⁰C. Cohen-Tannoudji and J. Dupont-Roc, *Phys. Rev. A* **5**, 968 (1972).
- ³¹R. Jiménez-Martínez, S. Knappe, and J. Kitching, *Rev. Sci. Instrum.* **85**, 045124 (2014).
- ³²W. Happer and B. S. Mathur, *Phys. Rev.* **163**, 12 (1967).
- ³³W. L. Wiese, M. W. Smith, and B. Glennon, *Atomic Transition Probabilities, Hydrogen through Neon Vol. I* (National Bureau of Standards, 1966).
- ³⁴C. Guttin, "Etude et réalisation d'un magnétomètre à hélium 4 pompé par laser à haute résolution et isotrope," Ph.D. thesis, Université Grenoble I, Grenoble, 1995.
- ³⁵F. Bloch and A. Siegert, *Phys. Rev.* **57**, 522 (1940).